Virtual Experiments via LSM for Quantitative 2-D Inverse Scattering: Challenges and Opportunities

Martina Teresa Bevacqua, *Member, IEEE*, and Loreto Di Donato, *Senior Member, IEEE*

***Abstract*— In this article, we investigate the virtual experiments (VE) setting by means of analytical solution of the far-field equation, that is the equation underlying the linear sampling method. In particular, an analytical expression for the internal field is derived in case of penetrable circular cylinders, which provides a straightforward and more comprehensive overview of the VE settings with particular hints on its reliability and validity range when applied for quantitative imaging. Numerical examples are reported to show the analytic findings, also in case of noncircular targets. The reported analysis can open the way to new possibilities in VE design for electromagnetic inverse scattering, microwave imaging, and related focusing problems.**

***Index Terms*— Far-field equation (FFE), field focusing, inverse scattering, linear sampling method (LSM), microwave imaging, virtual experiments (VE).**

I. Introduction and Motivations

ELECTROMAGNETIC inverse scattering represents an open issue in antennas and propagation community since it entails solution of a nonlinear and ill-posed problem. On the other hand, it is relevant in several applications, ranging from medical to subsurface imaging, civil surveillance, and nondestructive evaluation [1], which require reliable, computational efficient, and effective solution approaches. Different strategies have been proposed over the last years to address such a problem, mainly concerned with local and global optimization approaches, quantitative and qualitative strategies [2], and, lately, artificial intelligence and deep learning [3]. In this respect, one of the main effort has been devoted to reduce the so-called "degree of nonlinearity" by means of effective manipulation and smart rewritings of the basic equations. Some interesting examples include, but are not limited to, contrast source extended born model [4], subspace optimization method [5], Y0 model [6], and the family of new integral scattering equations [7].

Following this way, in a body of papers over the last decade, a new paradigm for solving the 2-D inverse scattering problem has been proposed. Such a paradigm stems for recasting the original scattering experiments into new virtual, software defined, ones without requiring any additional measurements. This can be actually pursued by means of a proper design equation which is able to condition the spatial behavior of the internal field or of the contrast source (i.e., the considered auxiliary unknown of the problem). Then, such a relevant conditioning can be conveniently exploited to introduce new inversion strategies. Some inversion approaches are discussed in [8], [9], [10], [11], and [12] and rely on the design of virtual experiments (VE) enforcing circular symmetric contrast sources (or total fields) for a set of points, called *pivot* points, through the solution of the far-field equation (FFE) [13]. VE-based inversion approaches show a great capability in imaging targets which do not belong to the so-called weak scattering approximations based on born approximation (BA) [14], while addressing the problem in a simple, effective, and computationally efficient way. On the other hand, their performance gets worse when targets' dimension and dielectric contrast become larger and larger. This circumstance has been partially analyzed in [15] through a simple numerical analysis, wherein an applicability range of about three times larger than BA has been found.

In order to better understand the reasons of the performance's worsening, in this article, we study analytically the FFE in case of penetrable circular cylinders under the 2-D transverse magnetic (TM) formulation to derive a direct expression for the internal field (or contrast source). This analytical expression, which depends on the target's contrast and on the considered pivot point, provides straightforward outcomes which fully agree with results of previous works on linear sampling method (LSM) and FFE interpretation [16], [17], [18]. More interestingly, the analytic expression allows also to understand why the VE-based inversion methods get worse performance beyond a given range of validity and may suggest some counteracting strategies to avoid their performance degradation.

The article is structured as follows. In Section II, the mathematical formulations of the problem and the FFE solution are introduced for the canonical case of a dielectric circular cylinder. In Section III, the analytic expression of the virtual total field is derived, while in Section IV, the main outcomes are discussed. Then, in Section V, a numerical analysis is

Manuscript received 12 October 2023; accepted 25 February 2024. Date of publication 21 March 2024; date of current version 7 May 2024. This work was supported in part by the European Union through the Italian National Recovery and Resilience Plan (NRRP) of NextGenerationEU, Partnership on "Telecommunications of the Future" (Program "RESTART") under Grant PE0000001. *(Corresponding author: Loreto Di Donato.)*

Martina Teresa Bevacqua is with the Department of Information Engineering, Infrastructures and Sustainable Energy, University "Mediterranea" of Reggio Calabria, 89124 Reggio di Calabria, Italy, and also with Consorzio Nazionale Interuniversitario per le Telecomunicazioni (CNIT), 43124 Parma, Italy (e-mail: martina.bevacqua@unirc.it).

Loreto Di Donato is with the Department of Electrical, Electronics and Computer Engineering, University of Catania, 95123 Catania, Italy, also with Consorzio Nazionale Interuniversitario per le Telecomunicazioni (CNIT), 43124 Parma, Italy, and also with the Laboratori Nazionali del Sud of the Istituto Nazionale di Fisica Nucleare, 95123 Catania, Italy (e-mail: loreto.didonato@unict.it).

Color versions of one or more figures in this article are available at https://doi.org/10.1109/TAP.2024.3378005.

Digital Object Identifier 10.1109/TAP.2024.3378005

performed to validate the previously derived analytic findings, while Section VI is instead focused on their exploitation in the framework of a VE-based linear inverse recovery approach. Discussion and Conclusions follow. Throughout the paper, the time harmonic factor $exp(j\omega t)$ is assumed and dropped.

II. Analytic Solution of the FFE for Circular Dielectric Cylinder

Let us consider an infinitely long and lossless circular cylinder of radius a along the z axis with complex relative permittivity ϵ_s. A TM incidence by plane waves with incoming direction $\theta_i \in [0, 2\pi]$ is assumed for the following analysis. The corresponding scattered field is collected in the far-field zone of the cylinder over a circular observation domain of radius R_o at different angular observation points $\theta_o \in [0, 2\pi]$. Under the above assumptions, the scattered field can be factored as

$$E_s(R_o, \theta_o, \theta_i) = \frac{e^{-\jmath k_0 R_o}}{\sqrt{R_o}} E_s^{\infty}(\theta_o, \theta_i) \tag{1}$$

where E_s^{∞} is the far-field pattern, $k_0 = \omega\sqrt{\epsilon_0\mu_0}$ is the background wavenumber (free space is assumed herein for the sake of simplicity), ω is the angular frequency, ϵ_0 and μ_0 are the free-space dielectric permittivity and magnetic permeability, respectively.

According to [19], the scattered field pattern E_s^{∞} and the transmitted field E_t, outside and inside the cylinder, respectively, can be analytically expressed through the following modal expansions

$$E_s^{\infty}(\theta_o, \theta_i) = \sqrt{\frac{2j}{\pi k_0}} \sum_{n=-\infty}^{+\infty} c_n e^{jn(\theta_o - \theta_i)} \tag{2}$$

$$E_t(\underline{r}, \theta_i) = \sum_{n=-\infty}^{+\infty} a_n J_n(k_s r) e^{jn(\theta_r - \theta_i)} \tag{3}$$

wherein $\underline{r} = (r\cos\theta_r, r\sin\theta_r)$ is the position vector, and the expansion coefficients are given by

$$c_n = \frac{J_n'(k_0 a) J_n(k_s a) - \sqrt{\epsilon_s} J_n(k_0 a) J_n'(k_s a)}{\sqrt{\epsilon_s} J_n'(k_s a) H_n^{(2)}(k_0 a) - J_n(k_s a) H_n^{'(2)}(k_0 a)} \tag{4}$$

and

$$a_n = j^{-n} \frac{J_n(k_0 a) H_n^{'(2)}(k_0 a) - J_n'(k_0 a) H_n^{(2)}(k_0 a)}{J_n(k_s a) H_n^{'(2)}(k_0 a) - \sqrt{\epsilon_s} J_n'(k_s a) H_n^{'(2)}(k_0 a)}. \tag{5}$$

In the expressions (4) and (5), $k_s = \omega\sqrt{\epsilon_s\epsilon_0\mu_0} = k_0\sqrt{\epsilon_s} = k_0\sqrt{1+\chi}$, being χ the contrast function defined as the difference between the complex relative permittivity of the cylinder and the one of the background medium [2]. Moreover, $H_n^{(2)}$ is the nth-order second kind Hankel function, J_n is the Bessel functions of nth-order and first kind, and the superscript $'$ denotes the derivative with respect to the argument. It is important to note that, as only a finite number of terms in (2) and (3) plays a role in the composition of the total field, the series can be truncated according to the rule of thumb $N_0 \approx k_0 a$ for (2) and $N_s \approx k_s a$ for (3), respectively.

In this framework, the LSM amounts to sense the investigation domain by sampling it into a set of points $\underline{r}_s = (r_s\cos\phi_s, r_s\sin\phi_s)$ and by solving the following equation

$$\mathcal{F}\left[i(\theta_i, \underline{r}_s)\right] = f(\theta_o, \underline{r}_s) \tag{6}$$

wherein $\mathcal{F}[\cdot]$ is the so-called far-field operator, $i(\theta_i, \cdot)$ the problem unknown, and $f(\theta_o, \underline{r}_s)$ the far-field pattern of a line source placed in the sampling points $\underline{r}_s$. The far-field operator is the angular pattern of the scattered field when collected under a multiview-multistatic configuration as defined in (2), while the right-hand side of (6) reads as

$$f(\theta_o, \underline{r}_s) = \sqrt{\frac{2j}{\pi k_0}} e^{jk_0 r_s cos(\theta_o - \theta_s)}. \tag{7}$$

Since $\mathcal{F}$ is a compact operator, solution of (6) must be pursued by means of a proper regularization strategy [13]. In this respect, singular value decomposition (SVD) and Tikhonov regularization can be exploited to get stable and reliable results [8]. Then, the support of the scatterer can be effectively retrieved by associating to the target's support those sampling points wherein the solution norm $||i||_{L^2}$ attains the lowest values with respect to its overall dynamic in the investigated region [13].

On the other hand, in case of circular cylinder, an analytical solution of the FFE can be achieved expanding the problem unknown in Fourier series. By doing so, as shown in [20], the latter can be expressed as

$$\begin{aligned} i(\theta_i, \underline{r}_s) &= \sum_{n=-\infty}^{+\infty} i_n(\underline{r}_s) e^{jn\theta_i} \\ &= \sum_{n=-\infty}^{+\infty} \left[\frac{1}{2\pi}\frac{1}{c_n} j^n J_n(k_0 r_s) e^{-jn\theta_s}\right] e^{jn\theta_i}. \end{aligned} \tag{8}$$

In [13], solution (8) has been proposed to solve the inverse obstacle problem since its energy, when plotted over the sampled domain, is able to image the scatterer's support.

III. Analytic Expression of the Virtual Transmitted Field

The VE paradigm is based on the simple observation that, for a fixed contrast function, the relationship between the total field transmitted into the target and the incident field holds linear. This circumstance entails that the original scattering experiments can be rearranged in a possibly more convenient form by means of a linear superposition of the incident fields [8], [9], [10], [11]. As a result, properly designed VE can give rise to total fields (or induced currents) exhibiting some useful properties which can be conveniently exploited in the recovery stage. In particular, the idea to design-specific VE enforcing total fields which are focused or exhibit a circular symmetry in the neighborhood of a "pivot" point has paved the way to a number of effective solution approaches for quantitative inverse scattering [8], [9], [10], [11]. It is also worth to underline that some other possibilities can be exploited to design VE, such as, for example, the factorization method (FM) [21] and the orthogonality sampling method

(OSM) [22], but these latter are out of the scope of the present paper.

From a mathematical point of view, a virtual incident field $\mathcal{E}_i$ can be simply obtained through a linear superposition of the original incident fields E_i through the FFE solution evaluated in a pivot point $\underline{r}_p$ belonging to the support of the target, i.e.,

$$\mathcal{E}_i(\underline{r}, \underline{r}_p) = \int_{-\pi}^{\pi} i(\theta_i, \underline{r}_p) E_i(\underline{r}, \theta_i) d\theta_i. \tag{9}$$

Then, the virtual total field $\mathcal{E}_t$ transmitted inside the cylinder can be expressed as superposition of the original ones E_t by means of the same coefficients $i(\theta_i, \underline{r}_p)$, i.e.,

$$\mathcal{E}_t(\underline{r}, \underline{r}_p) = \int_{-\pi}^{\pi} i(\theta_i, \underline{r}_p) E_t(\underline{r}, \theta_i) d\theta_i. \tag{10}$$

In order to investigate the expression of the virtual total field, let us substitute $i(\theta_i, \underline{r}_p)$ given by (8) into (10). Then, by changing the order of the integral and the sum, and substituting the expression of the original total field in (3), one gets

$$\mathcal{E}_t(\underline{r}, \underline{r}_p) = \sum_{m=-\infty}^{+\infty} a_m J_m(k_s r) e^{jm\theta_r} \sum_{n=-\infty}^{+\infty} i_n(\underline{r}_s) \int_{-\pi}^{\pi} e^{-j(m-n)\theta_i} d\theta_i. \tag{11}$$

Finally, by exploiting the orthogonality relation between the above exponential functions, the following expression can be obtained

$$\mathcal{E}_t(\underline{r}, \underline{r}_p) = \sum_{m=-\infty}^{+\infty} b_m J_m(k_s r) J_m(k_0 r_p) e^{jm(\theta_r - \theta_p)} \tag{12}$$

wherein $b_m = (a_m / c_m)$.

Interestingly, when $\underline{r}_p = (0, 0)$, the only term which survives in the expression (12) is the one for $m = 0$ as the $J_m(0) = 0$ for $m \neq 0$. Then, the VE total field induced in the cylinder is exactly a Bessel function of zero order apart from the constant b_0.

On the other hand, when $\underline{r}_p \neq (0, 0)$, one has to consider the behavior of the expansion coefficients. In particular, if the coefficients b_m are constant with respect to the order m (at least for the first relevant terms in the sum), the above expression can be further simplified by exploiting the Graf's addition theorem for the Bessel functions [23], i.e.,

$$\mathcal{E}_t(\underline{r}, \underline{r}_p) \approx b_0 \sum_{m=-\infty}^{+\infty} J_m(k_s r) J_m(k_0 r_p) e^{jm(\theta_r - \theta_p)} = b_0 J_0\left(k_s \left| \underline{r} - \frac{\underline{r}_p}{\sqrt{1+\chi}} \right|\right). \tag{13}$$

The above expression states that the virtual total field can be approximated (apart from an unessential constant factor) by a 0th-order Bessel function. Then, the virtual total field exhibits a circular symmetry and is also focused, but not simply with respect to the pivot point $\underline{r}_p$, as one would expect from the cylindrical pattern enforced by the right-hand-term of the FFE. Indeed, a rigid translation of the focusing point, i.e., the point where the 0th-order Bessel function attains its maximum, is introduced due to the scale factor $(\sqrt{1+\chi})^{-1}$.

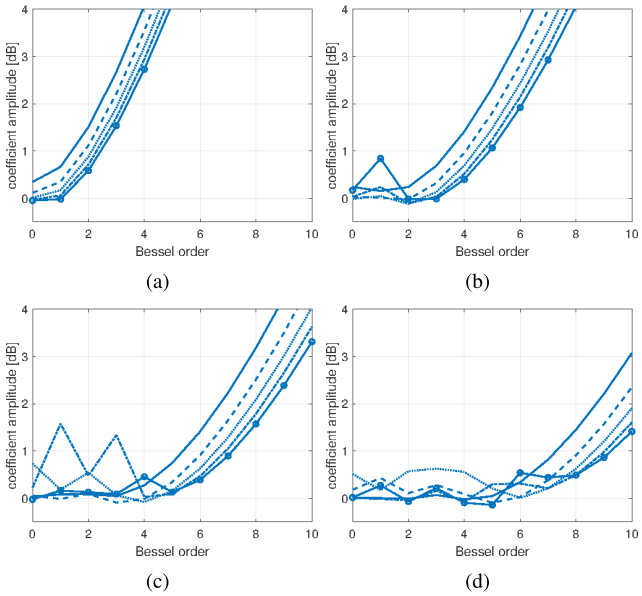

Fig. 1. Plots of coefficients (A.3) for different cylinder radii and different values of ϵ_s in the range [1.5–3.5]. (a) $0.25\lambda_b$. (b) $0.5\lambda_b$. (c) $0.75\lambda_b$. (d) $1\lambda_b$. The solid line corresponds to $\epsilon_s = 1.5$, dashed line $\epsilon_s = 2$, dotted line $\epsilon_s = 2.5$, dashed-dotted line $\epsilon_s = 3$, and circular markers solid line $\epsilon_s = 3.5$.

TABLE I
SYNTHETIC PARAMETER *symcirc* AS A FUNCTION OF RELATIVE PERMITTIVITY ϵ_s IN CASE OF $\underline{r}_p = (0.125\lambda_b, 0.216\lambda_b)$

ϵ_s	$symcirc(\mathcal{E}_t)$	$symcirc(J_0)$	*shift* $[\lambda_b]$
1.5	7.92	6.65	0.045
2	12	7.48	0.073
2.5	19.6	7.76	0.091
3	28.1	7.56	0.10
3.5	41	7	0.12

Finally, if the coefficients b_m are not constant with respect to the order m (at least for the first relevant terms of the sum), a total field distribution resembling a Bessel function is not guaranteed, as it will be shown in Sections IV and V.

IV. EXPECTED PROPERTIES OF THE VIRTUAL TRANSMITTED FIELD

The approximation (13) derived in the previous section allows to gain a deep understanding of the expected spatial distribution of the virtual transmitted field.

First of all, the larger the contrast, the larger the shift of the actual focusing point from the relevant pivot point $\underline{r}_p$. This implies that the use of the FFE to design circularly symmetric VE is expected to work worsen and worsen for increasing optical density of the target. In particular, for any arbitrary contrast value and electrical dimension of the scatterer, the VE internal fields corresponding to the outermost pivot points are affected by a larger shift than the internal ones. This entails that, for low contrast extended targets, the shift of the focusing point is also expected to be larger and larger for the outermost pivot points. Conversely, there are only two circumstances for which the shift is irrelevant. For $\chi = 0$ the shift would be exactly null, however, this circumstance is not in order since the scattered field would be null. Instead, more interestingly, the shift is null also for the pivot point pertaining to the cylinder's center.

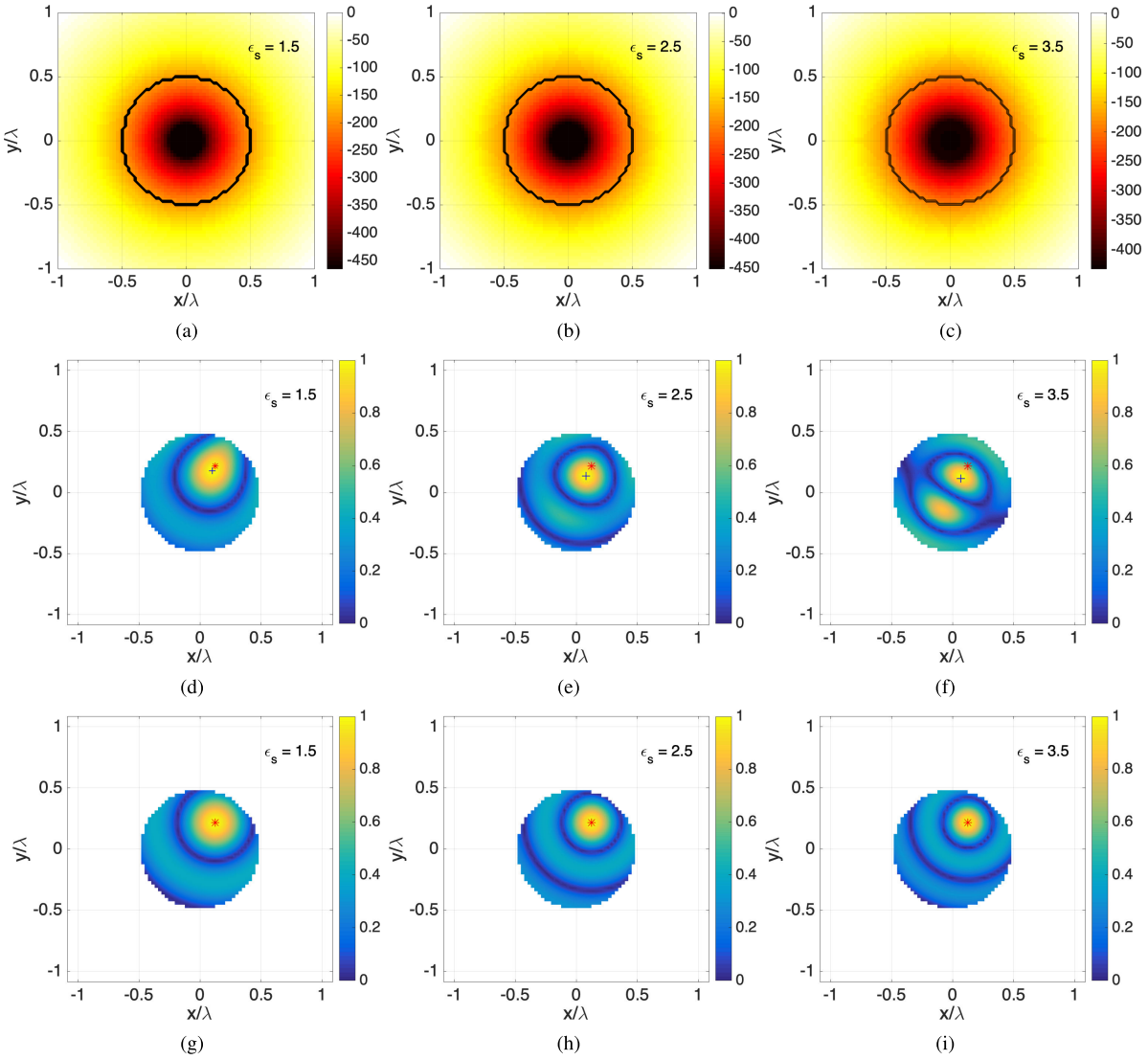

Fig. 2. Numerical analysis in case of $\underline{r}_p = (0.125\lambda_0, 0.216\lambda_0)$. (a)–(c) LSM spatial indicators with superimposed the contour of the target support. Subplots (d)–(f) show amplitudes of the normalized VE total fields induced within the circular targets; subplots (g)–(i) show the pertaining Bessel functions J_0 focused in the considered pivot point. This latter is superimposed as red asterisk, while the actual focusing point, shifted according to (13), is shown with a black cross.

Another important role for the internal field behavior is played by the expansion coefficients b_m. Indeed, as mentioned above, if the coefficients b_m are constant with respect to m, the Graf's theorem can be invoked and the internal field would be exactly a Bessel function given by (13). By relaxing such an hypothesis, even when the coefficients b_m are all almost constant with m (at least up to the truncation index in the relevant series), the sum gives rise to a total field that can be approximated by (13) (within a given error). On the other hand, when the coefficients differ too much one from each other, the recombined total field will not resemble the Bessel function stated by the Graf's theorem.

In order to study the behavior of the expansion coefficients with respect to the dimension and dielectric constant of the cylinder, and their impact on the circular symmetry of the virtual internal field, we derive an explicit expression of such coefficients, which is reported in Appendix, see eqs. (A.1)–(A.3). Then, we plot the coefficients for different radius a and dielectric constant ϵ_s. As it can be seen in Fig. 1, the coefficients exhibit a finite value up to a given order m, which corresponds to the last relevant term in (12), while they grow to infinity beyond a given order m, that is when the integral in (A.3) goes to zero. For example, for the radius $0.25\lambda_b$, only the first two coefficients are relevant in series (12) and are almost equal one each other, even in case of largest contrast, see Fig. 1(a). When the radius increases, the dependence of the coefficients as a function of m becomes more complex for increasing values of the dielectric constant, see Fig. 1(b)–(d). Such an analysis suggests that for increasing value of the product $k_s a$ of the cylinder, the internal field cannot show a perfect circular symmetry with respect to the considered pivot point since its expression differs from the 0th-order Bessel function stated by the Graf's theorem.

V. Numerical Assessment

In this section, we show some numerical tests to better understand and discuss the findings of the previous Section. In particular, the main aim is to compare the actual VE

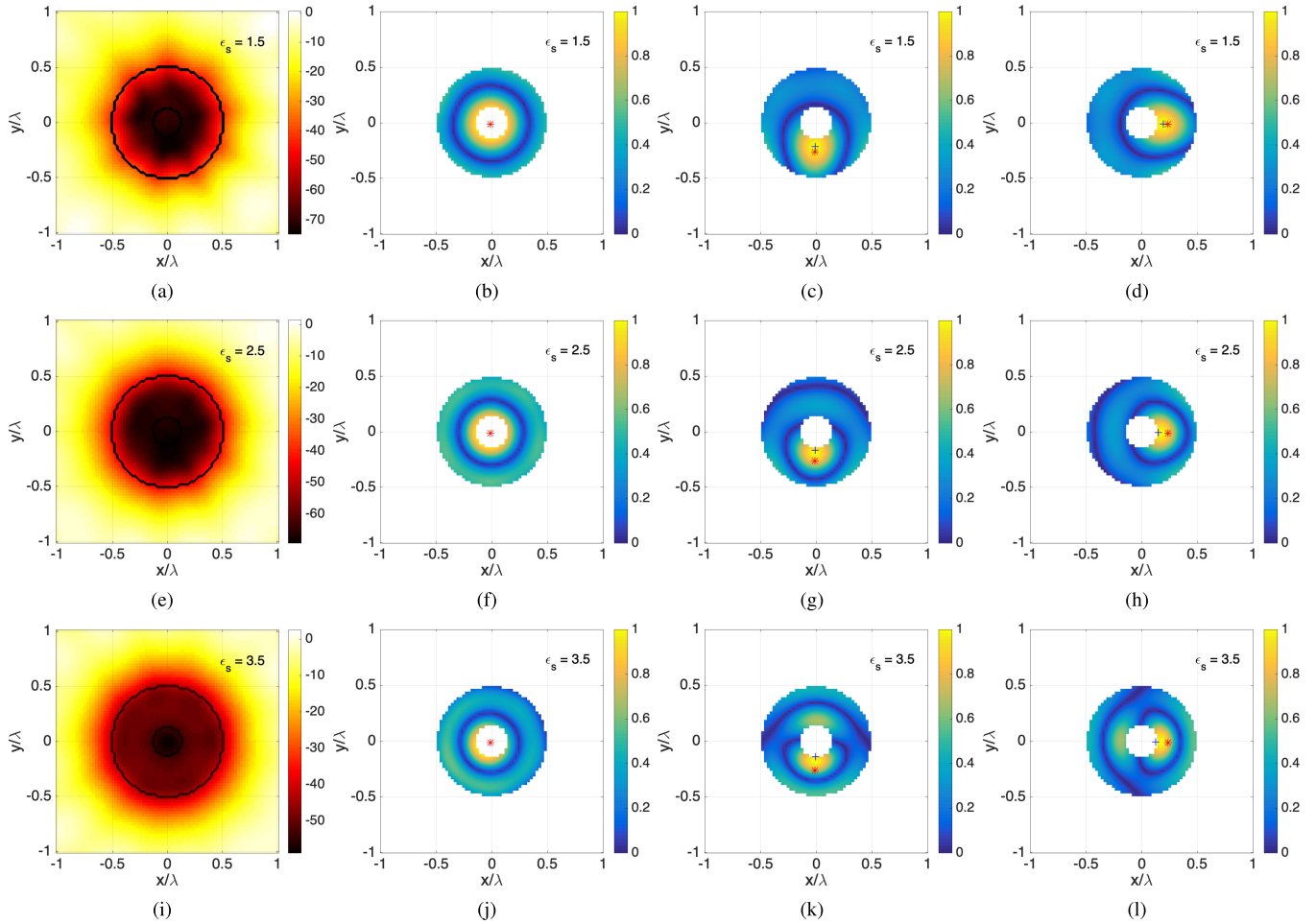

Fig. 3. Numerical analysis for ring target. (a), (e), (i) LSM spatial indicators with superimposed the contour of the target support. The subplots (b)–(d), (f)–(h), and (j)–(l) show the amplitudes of the normalized VE total fields induced within the circular target for different pivot points. The considered pivot points are superimposed as red asterisks, while the actual focusing points, shifted according to (13), are shown with black crosses.

transmitted field (12) and the Bessel function J_0, when both defined with respect to the same pivot point $\underline{r}_p$. The benchmark scenario consists of a lossless circle of radius $a = 0.5\lambda_0$ and different dielectric constants ϵ_s, embedded in free space within a square domain of side $L = 2.2\lambda_0$, which is discretized into 80 × 80 cells. Without loss of generality, we assume $\theta_m = \theta_i$. According to the Nyquist criterion underlying the degrees of freedom of scattered field suggested in [24], $N = M = 16$ incident directions and measurements have been considered. The scattered field data has been generated by means of analytical formulas given in [19]. Fig. 2 shows the amplitudes of the normalized virtual transmitted field designed by means (12) and the related Bessel function J_0, respectively. As it can be seen, the larger the relative permittivity ϵ_s, the larger the shift of the total field with respect to the pivot point $\underline{r}_p$ and the larger the deformation of the cylindrical wavefront for the internal field. Even, for $\epsilon_s = 3.5$ an undesired sidelobe appears in the internal field destroying completely the well-focused and cylindrical symmetry of the field pattern. This circumstance does not hold true when the pivot point is located at the center of the cylinder as analytically derived in the previous Section. Indeed, when the $\underline{r}_p = 0$ no shift of the field's maximum is observed, neither wavefront deformation, but a perfect circularity of the field distribution is ensured (the relevant plots are not shown for the sake of brevity). To quantitatively appraise the difference in term of circular pattern of the internal field, a synthetic parameter has been adopted. It is defined as the L^2-norm of the angular derivative ∂_{ϕ_r} of the virtual total field, that is

$$symcirc(\underline{r}_p) = \left\| \partial_{\phi_r} \left[\mathcal{E}_t(\underline{r}, \underline{r}_p) \right] \Pi(\underline{r}, \underline{r}_p) \right\|_2^2 \qquad (14)$$

wherein ϕ_r is the angular coordinate of a local polar reference system centered in $\underline{r}_p$ and $\Pi(\underline{r}, \underline{r}_p)$ identifies the minimum circle centered on $\underline{r}_p$ inscribed in the target. The larger the value of $symcirc$, the worse the circular symmetry around the considered pivot point. As it can be seen from Table I, the higher the relative permittivity ϵ_s, the worse the cylindrical symmetry of the field in terms of the adopted metric. Only in case of $\epsilon_s = 1.5$, the $symcirc$ of the virtual field is comparable to the one of the Bessel function.

In order to show that the above findings hold true also for targets other than the circular ones, a kite and a ring shaped targets have been considered. The targets are embedded in a square domain with size of 2λ, discretized with 80 × 80 number of cells. The leading dimension of both targets is 1λ. To probe the targets, 21 plane waves and 21 measurement points are considered, the latter located uniformly over the circle with radius $R = 10\lambda$. The synthetic scattered fields

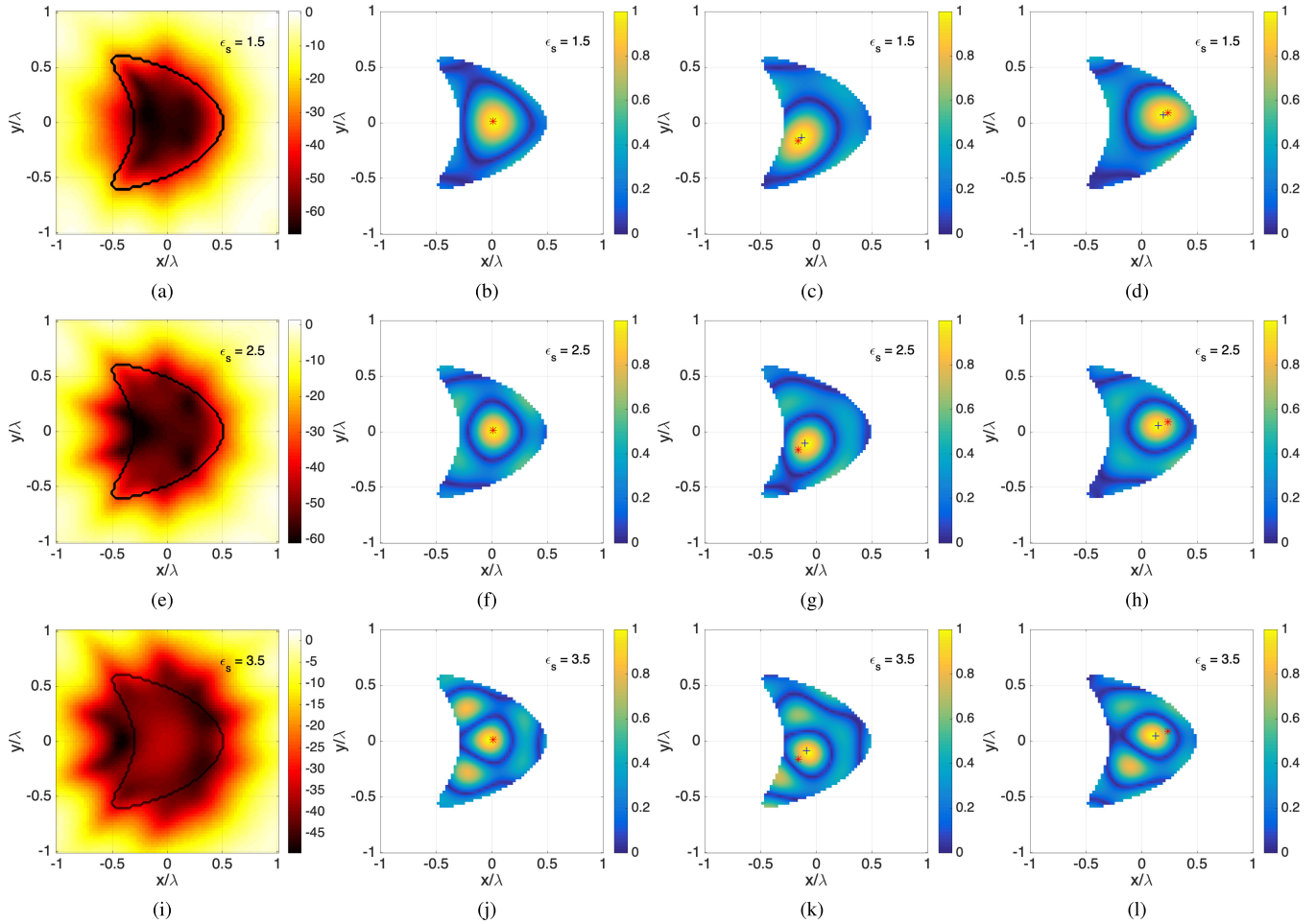

Fig. 4. Numerical analysis for kyte target. (a), (e), (i) LSM spatial indicators with superimposed the contour of the target support. The subplots (b)–(d), (f)–(h), and (j)–(l) show the amplitudes of the normalized VE total fields induced within the circular target for different pivot points. The considered pivot points are superimposed as red asterisks, while the actual focusing points, shifted according to (13), are shown with black crosses.

TABLE II
PERFORMANCE INDICATOR TO EVALUATE THE BEHAVIOR OF THE EXPANSION COEFFICIENTS (A.3)

$I = k_0\sqrt{\epsilon_s}a$				
	0.25λ	0.5λ	0.75λ	1.0λ
$k_0\sqrt{1.5}$	1.92	3.85	5.77	7.70
$k_0\sqrt{2.0}$	2.22	4.44	6.66	8.89
$k_0\sqrt{2.5}$	2.48	4.97	7.45	9.93
$k_0\sqrt{3.0}$	2.72	5.44	8.26	10.88
$k_0\sqrt{3.5}$	2.94	5.88	8.82	11.75

have been numerically evaluated by using a full-wave forward solver based on the method of moments [25] and organized into a complex matrix (with size of 21 × 21), while the FFE equation has been solved numerically by adopting the Tikhonov regularization [8]. Results are shown in Figs. 3 and 4. Even if the targets are not circular cylinders and some possible deformations of the internal fields can be due to the geometrical shape, the trend observed in Fig. 2 for the circular cylinder is still confirmed.

VI. EXPLOITATION OF THE OUTCOMES THROUGH A LINEAR INVERSION APPROACH

In this section, the inversion results within the framework of a VE based linear inversion approach [8] are reported in order to assess the outcomes of the derived analysis. The reconstructions of the cylinder and kite targets are discussed and shown with and without the shift compensation of the pivot points foreseen by (13). Of course, it is possible to compensate this shift when the target contrast ϵ_s is approximately known. In the following, ϵ_s is assumed known, in order to check if the shift compensation can have an impact on the final reconstruction.

The region of interest has been probed by means of $N = 19$ angular equally spaced plane waves and the scattered field is collected at $M = 19$ points all around the investigation domain at a distance of 4λ from the center of the reference system. Finally, the scattered field has been corrupted by additive white Gaussian noise with a SNR = 25 dB. The reader is referred to [8] for details about the linear reconstruction approach. A standard truncated SVD has been selected to solve the relevant ill-posed linear problem, wherein the cutoff value in the reconstruction formula is chosen according to the Picard's plot [26].

The first test bench is a perfect lossless cylindrical target with radius 0.6λ and dielectric constant 1.75, see Fig. 5(a). In Fig. 5(b)–(e), the set of pivot points without and with shift compensation and the relevant reconstruction of the target are reported, respectively. For the sake of brevity, the imaginary

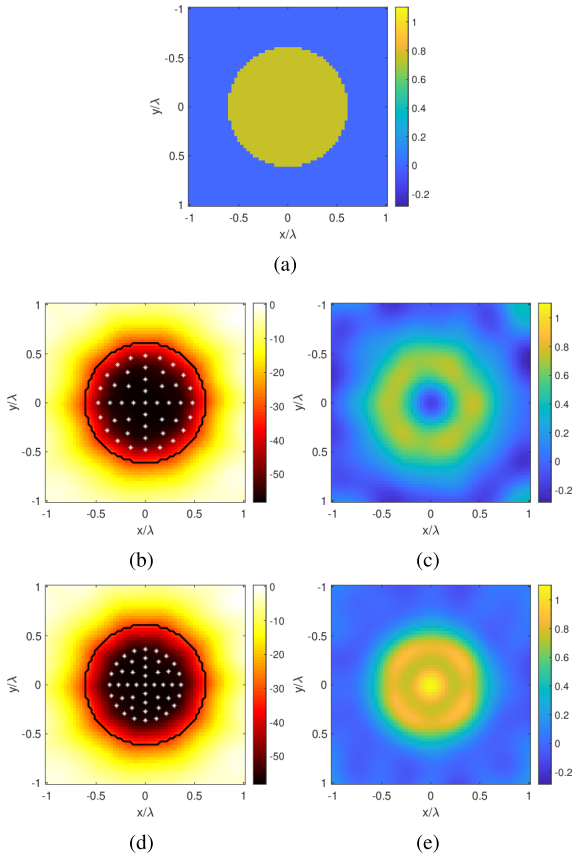

Fig. 5. Reconstruction of a cylinder with radius 0.6λ and dielectric constant 1.75. (a) Ground truth. (b) LSM map with superimposed the original pivot points. (c) TSVD reconstruction with pivot points shown in (b), the NMSE is $err = 27\%$. (d) LSM map with superimposed the compensated pivot points shifted according to (13), (e) TSVD reconstruction with shift compensantion, the NMSE is $err = 9\%$.

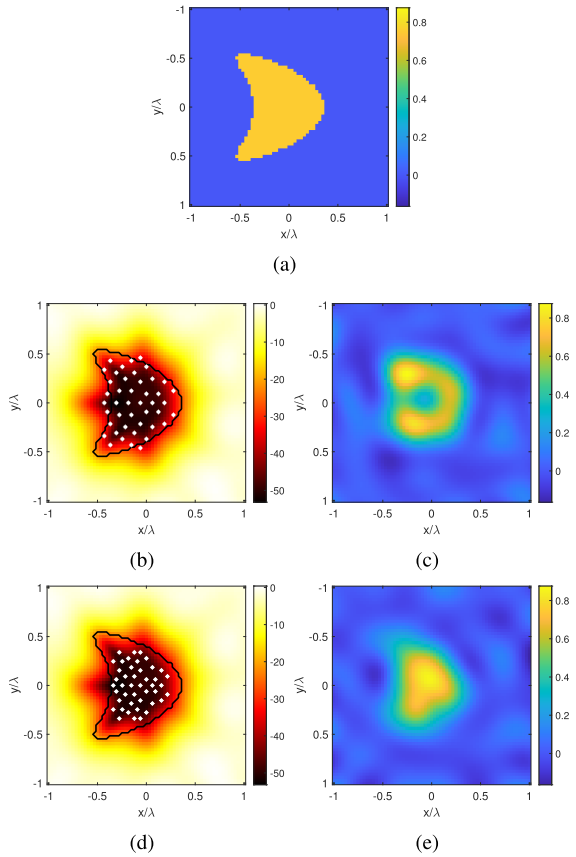

Fig. 6. Reconstruction of a kite target with dielectric constant 1.75. (a) Ground truth. (b) LSM map with superimposed the original pivot points. (c) TSVD reconstruction with pivot points shown in (b), the NMSE is $err = 28\%$. (d) LSM map with superimposed the compensated pivot points shifted according to (13). (e) TSVD reconstruction with shift compensantion, the NMSE is $err = 24\%$.

part is not reported being negligible with respect to the real one. As it can be seen, the reconstruction achieved by shift compensation is more accurate and the normalized mean square error (NMSE) attains lower values (see details in the figure's caption).

The second example is a noncircular scatterer, i.e., the kite with a leading dimension of 1λ. Also in this case, the shift compensation of the pivot points allows to achieve a better reconstruction, without holes in the central part of the scatterer and a lower reconstruction error, see Fig. 6. In this case, it is worth to notice that some pivot points are not taken exactly within the scatterer's support because the LSM map does not exactly resemble the actual target's shape due to concavity of the kite [27]. Anyway, the reconstruction is quantitative although slightly underestimates the actual dimension of the target.

As a final comment, it is worth to underline that the developed analysis is only a proof of concept as the exact shift of the pivot points is not known in any actual instances, depending on turn of the local value of the contrast. However, in the light of future developments, the value of the contrast can be estimated by other auxiliary techniques or in distorted approaches, wherein the shift compensation can be refined at each step of the iterative procedure.

VII. Discussion and Conclusion

In this article, an analytical expression for the VE internal field has been derived, able to describe the virtual transmitted field designed via LSM. The developed analysis reveals several interesting features which allow a deeper understanding of the design equation used for the VE paradigm.

First of all, outcomes of (12)–(13) show that, if the expansion coefficients can be assumed (approximately) constant up to the truncation index, the internal field resembles the cylindrical symmetry of the Bessel function of zero order, but for a shift of the focusing point which can be assumed negligible only for low contrast and/or small targets.[1] This result is quite well in agreement with the physical interpretation of the LSM in terms of focusing strategy given in [16]. On the other hand, the focusing interpretation is no longer valid when the scatterer shows larger and larger contrast, since the expansion coefficients in (12) cannot be assumed constant with m. Interestingly, such circumstance is also numerically shown in the framework of a linearized VE based reconstruction approach proposed in [15], wherein the indicator[2] proposed to appraise the validity of the method amounts to 3.85, which

[1]The targets we are considering as low contrast in the context of this article are anyway beyond the scattering regime concerned with BA [28].

[2]In [15] the indicator is formulated with respect to the circle's diameter rather than the radius as in this paper.

is the value reported in Table II for a radius of 0.5λ and dielectric constant $\epsilon_s = 1.5$. The numerical analysis suggested by the analytical findings fully agrees with the one reported in [15].

It is also interesting to discuss the implication of the analytical findings in the light of the results provided by [17], wherein it is shown that the L^2-norm of (8) diverges for all sampling points different from the sampling point at the center of the cylinder. The present analysis also identifies such a peculiar point because it is the only one which ensures exact circular symmetry of the internal field, whatever the amplitude and size of the scatterer. Instead, in all the other pivot points, the internal field cannot exactly match a cylindrical focused pattern and needs to increase its energy by involving nonradiating currents [29].

Finally, the obtained results are also in agreement with the discussion in [18], wherein it is shown that a circular symmetric pattern can be also radiated by any arbitrary shaped source, not necessarily a circular or mainly focused one, owing to the occurrence of nonradiating currents [29]. Indeed, also not focused internal fields are compatible with the FFE solution as shown in Fig. 2(f).

However, it is important to note that when the regularization scheme is considered, the nonradiating currents are minimized and the radiating ones are predominant and are expected to be circularly symmetric as discussed in [16]. This circumstance allows to interpret the LSM as nearly optimal focusing strategy in the neighborhood of the pivot point [16], [30].

On the other hand, both the shift of the focusing point and the deformation of the cylindrical wave pattern explain, in a straightforward manner, the reason why the performance of LSM based VE recovery strategies worsen in imaging strong scatterers with leading dimension larger than λ_0. For instance, the shift of the focusing point can prevent the accuracy of the underlying source point field approximation in the linearized inversion method [8], as shown by means of the examples in Section VI. Furthermore, in [9], the penalty term enforcing circular symmetry of the contrast sources with respect to the pivot points could not act properly in case of significant deformation and shift of the cylindrical field pattern. Finally, in [11], the algebraic approach could not work properly since the polynomial expansion of the Bessel function around the pivot point would be not properly exploited.

It is also worth noticing that (13) can suggest some counteracting strategies to avoid performance degradation of the VE. For instance, a proper compensation procedure could be adopted to correct the actual focusing point as shown in Section VI. Last but not least, results in case of strong targets show that total field distributions other than circular ones could be sought, so they suggest the use of different design equations to enlarge the class of retrievable scatterers by means of VE inversion strategies [31].

A last comment must be spent to discuss the extension to the more realistic case concerned with the 3-D problem. In this respect, it is worth to recall that the VE framework up to now has been introduced and discussed only for 2-D scalar problem. In order to extend and tailor the VE framework to the more challenging 3-D case, two possibilities can be of interest. The first one is concerned with scalar fields, such as acoustic waves, wherein the problem still holds scalar and the rationale underlying VE and the above analytical developments can be extended and tailored. Conversely, for vector fields, the VE design entails the finding of the optimal polarization as additional problem's degree of freedom [32]. Then, one could split the problem as three scalar separate focusing problems by considering three different independent polarizations and recasting the problem accordingly. Also in this case, the extension of the suggested analysis are expected to help in gaining more insights into the VE settings.

APPENDIX

In this Appendix, the analytical expression of the coefficients ratio b_m in expansion (12) is derived. By recalling the expressions (4)–(5) and substituting in b_m, a compact expression can be obtained

$$b_m = \frac{J_m(k_0a)H_m^{(2)'}(k_0a) - J_m'(k_0a)H_m^{(2)}(k_0a)}{\sqrt{\epsilon_s}J_m(k_0a)J_m'(k_sa) - J_m'(k_0a)J_m(k_sa)}. \quad \text{(A.1)}$$

Then, substituting the expression for the Hankel function and its first derivative ($H_m^{(2)} = J_m - jY_m$ and $H_m^{(2)'} = J_m' - jY_m'$), recalling the Wronskian of the Bessel functions ($J_m(x)Y_m(x)' - Y_m(x)J_m'(x) = 2/\pi x$) and the recursive formula of the derivative of Bessel functions ($J'(\alpha x) = \alpha J_{m-1}(\alpha x) - (m/\alpha)J_m(\alpha x)$), the following ultimate expressions for b_m can be obtained

$$b_m = \frac{\left(\frac{-2_J}{\pi k_0 a}\right)}{\sqrt{\epsilon_s}J_m(k_0a)J_{m-1}(k_sa) - J_{m-1}(k_0a)J_m(k_sa)}. \quad \text{(A.2)}$$

Further manipulations can be performed by means of the expression (6.521) in [33] to obtain

$$b_m = \frac{2_J}{\pi(k_0a)^2\chi\int_0^1 \rho J_m(k_0a\rho)J_m(k_sa\rho)d\rho} \quad \text{(A.3)}$$

wherein ρ is the radial variable spanning the unitary disk. The above expression of b_m has a more straightforward readability than the previous ones.

ACKNOWLEDGMENT

The authors would thank Prof. T. Isernia and Dr. L. Crocco for their fruitful discussions, and Prof. R. Pierri for his stimulating incentives, about this topic in the last recent years.

REFERENCES

[1] M. Pastorino and A. Randazzo, *Microwave Imaging Methods and Applications*. Norwood, MA, USA: Artech House, 2018.
[2] M. Pastorino, *Microwave Imaging*. Hoboken, NJ, USA: Wiley, 2010.
[3] X. Chen, Z. Wei, M. Li, and P. Rocca, "A review of deep learning approaches for inverse scattering problems (invited review)," *Prog. Electromagn. Res.*, vol. 167, pp. 67–81, 2020.
[4] T. Isernia, L. Crocco, and M. D'Urso, "New tools and series for forward and inverse scattering problems in lossy media," *IEEE Geosci. Remote Sens. Lett.*, vol. 1, no. 4, pp. 327–331, Oct. 2004.
[5] X. Chen, "Subspace-based optimization method for solving inverse-scattering problems," *IEEE Trans. Geosci. Remote Sens.*, vol. 48, no. 1, pp. 42–49, Jan. 2010.
[6] M. T. Bevacqua and T. Isernia, "An effective rewriting of the inverse scattering equations via Green's function decomposition," *IEEE Trans. Antennas Propag.*, vol. 69, no. 8, pp. 4883–4893, Aug. 2021.

[7] Y. Zhong, M. Lambert, D. Lesselier, and X. Chen, "A new integral equation method to solve highly nonlinear inverse scattering problems," *IEEE Trans. Antennas Propag.*, vol. 64, no. 5, pp. 1788–1799, May 2016.

[8] L. Crocco, I. Catapano, L. Di Donato, and T. Isernia, "The linear sampling method as a way to quantitative inverse scattering," *IEEE Trans. Antennas Propag.*, vol. 60, no. 4, pp. 1844–1853, Apr. 2012.

[9] L. Di Donato, M. Bevacqua, L. Crocco, and T. Isernia, "Inverse scattering via virtual experiments and contrast source regularization," *IEEE Trans. Antennas Propag.*, vol. 63, no. 4, pp. 1669–1677, Apr. 2015.

[10] L. Di Donato and L. Crocco, "Model-based quantitative cross-borehole GPR imaging via virtual experiments," *IEEE Trans. Geosci. Remote Sens.*, vol. 53, no. 8, pp. 4178–4185, Aug. 2015.

[11] M. T. Bevacqua, L. Crocco, L. Di Donato, and T. Isernia, "An algebraic solution method for nonlinear inverse scattering," *IEEE Trans. Antennas Propag.*, vol. 63, no. 2, pp. 601–610, Feb. 2015.

[12] Y. Gan, C. Yin, Q. Fan, and A. Li, "A fast inverse scattering imaging method by applying virtual experiments to T-matrix scheme," *IEEE Access*, vol. 8, pp. 195122–195131, 2020.

[13] D. Colton, H. Haddar, and M. Piana, "The linear sampling method in inverse electromagnetic scattering theory," *Inverse Problems*, vol. 19, no. 6, pp. 105–137, Dec. 2003.

[14] A. J. Devaney, "Geophysical diffraction tomography," *IEEE Trans. Geosci. Remote Sens.*, vol. GE-22, no. 1, pp. 3–13, Jan. 1984.

[15] L. Di Donato, R. Palmeri, G. Sorbello, T. Isernia, and L. Crocco, "Assessing the capabilities of a new linear inversion method for quantitative microwave imaging," *Int. J. Antennas Propag.*, vol. 2015, pp. 1–9, Aug. 2015.

[16] I. Catapano, L. Crocco, and T. Isernia, "On simple methods for shape reconstruction of unknown scatterers," *IEEE Trans. Antennas Propag.*, vol. 55, no. 5, pp. 1431–1436, May 2007.

[17] A. Liseno and R. Pierri, "Impossibility of recovering a scatterer's shape by the first version of the 'linear sampling' method," *Int. J. Electron. Commun.*, vol. 57, no. 1, pp. 70–73, Jan. 2003.

[18] K. Agarwal, X. Chen, and Y. Zhong, "A multipole-expansion based linear sampling method for solving inverse scattering problems," *Opt. Exp.*, vol. 18, no. 6, pp. 6366–6381, 2010.

[19] C. A. Balanis, *Advanced Engineering Electromagnetics*. Hoboken, NJ, USA: Wiley, 1989.

[20] A. Liseno and R. Pierri, "Imaging perfectly conducting objects as support of induced currents: Kirchhoff approximation and frequency diversity," *J. Opt. Soc. Amer. A, Opt. Image Sci.*, vol. 19, no. 7, pp. 1308–1318, 2002.

[21] L. Crocco, L. Di Donato, I. Catapano, and T. Isernia, "The factorization method for virtual experiments based quantitative inverse scattering," *Prog. Electromagn. Res.*, vol. 157, pp. 121–131, 2016.

[22] M. T. Bevacqua, R. Palmeri, T. Isernia, and L. Crocco, "A simple procedure to design virtual experiments for microwave inverse scattering," *IEEE Trans. Antennas Propag.*, vol. 69, no. 12, pp. 8652–8663, Dec. 2021.

[23] M. Abramowitz and I. Stegun, *Handbook of Mathematical Functions With Formulas, Graphs and Mathematical Tables*. New York, NY, USA: Dover, 1972.

[24] O. M. Bucci and T. Isernia, "Electromagnetic inverse scattering: Retrievable information and measurement strategies," *Radio Sci.*, vol. 32, no. 6, pp. 2123–2137, Nov. 1997.

[25] J. Richmond, "Scattering by a dielectric cylinder of arbitrary cross section shape," *IEEE Trans. Antennas Propag.*, vol. AP-13, no. 3, pp. 334–341, May 1965.

[26] P. C. Hansen, "The truncated SVD as a method for regularization," *BIT Numer. Math.*, vol. 27, pp. 354–553, Dec. 1987.

[27] L. Crocco, L. Di Donato, I. Catapano, and T. Isernia, "An improved simple method for imaging the shape of complex targets," *IEEE Trans. Antennas Propag.*, vol. 61, no. 2, pp. 843–851, Feb. 2013.

[28] M. Slaney, A. C. Kak, and L. E. Larsen, "Limitations of imaging with first-order diffraction tomography," *IEEE Trans. Microw. Theory Techn.*, vol. MTT-32, no. 8, pp. 860–874, Aug. 1984.

[29] A. J. Devaney and E. Wolf, "Radiating and nonradiating classical current distributions and the fields they generate," *Phys. Rev. D*, vol. 8, no. 4, pp. 1044–1047, Aug. 1973.

[30] L. Crocco, L. Di Donato, D. A. M. Iero, and T. Isernia, "An adaptive method to focusing in an unknown scenario," *Prog. Electromagn. Res.*, vol. 130, pp. 563–579, 2012.

[31] L. Di Donato, M. T. Bevacqua, A. F. Morabito, and T. Isernia, "Orbital angular momentum and virtual experiments for microwave imaging," in *Proc. Photon. Electromagn. Res. Symp.*, Jun. 2019, pp. 560–565.

[32] D. A. M. Iero, "Constrained power focusing in inhomogeneous media as a polarization optimization," *Int. J. Antennas Propag.*, vol. 2015, pp. 1–7, Jan. 2015.

[33] I. S. Gradshteyn and I. M. Ryzhik, *Table of Integrals, Series and Products*, A. Jeffrey, Ed. London, U.K.: Academic, 1997.

Martina Teresa Bevacqua (Member, IEEE) was born in Reggio Calabria, Italy, in 1988. She received the M.S. Laurea degree (hons) in electronic engineering and the Ph.D. degree in information engineering from the University Mediterranea of Reggio Calabria, Reggio Calabria, Italy, in July 2012 and May 2016, respectively.

She is currently working as an Associate Professor with the University Mediterranea of Reggio di Calabria. Her research interests include activity mainly concerns electromagnetic inverse problems, with particular interest in: 1) inverse scattering problems from both a theoretical and applicative point of view and 2) field intensity shaping in nonhomogeneous and unknown scenario for hyperthermia treatment planning, wireless power transfer, and MRI shimming.

Dr. Bevacqua was the recipient of the Barzilai Award from the Italian Electromagnetics Society in 2014, and Young Scientist Award by International Union of Radio Science (URSI AT-RASC 2018). Moreover, she received the Honorable Mention from IEEE-Antennas and Propagation Society (Central and Southern Italy Chapter) in the 2016 best Student Member paper competition. She was also the recipient of the Mojgan Daneshmand Grants by Antennas and Propagation Society (APS-URSI 2023) and again the Young Scientist award by International Union of Radio Science (EMTS 2023). Moreover, in November 2023 she received the "IEEE Antennas and Propagation Ulrich L. Rohde Best Innovative Conference Paper Awards on Antennas Measurements and Applications" at the 2023 IEEE International Conference on Antenna Measurements and Applications. From April 2023, she is also Vice-Chair of the IEEE Young Professional Affinity Group of the IEEE Italy Section.

Loreto Di Donato (Senior Member, IEEE) was born in Caserta, Italy, in 1983. He received the M.Sc. and B.Sc. Laurea degrees in biomedical engineering from the University of Naples "Federico II", Naples, Italy, in 2006 and 2008, respectively, and Ph.D. degree in information engineering from the University "Mediterranea" of Reggio Calabria, Reggio Calabria, Italy, in 2012.

In 2009, he joined the Institute for Electromagnetic Sensing of the Environment—National Research Council (IREA-CNR) of Italy in Naples with a research grant. Since 2013, he has been with the Department of Electrical, Electronics and Computer Engineering, University of Catania, Catania, Italy, where he is currently an Associate Professor of electromagnetic fields. His research interests include inverse scattering problems for microwave and mm-waves diagnostics, antenna array synthesis and focusing problems, bioelectromagnetics dosimetry and interactions at millimeter waves frequencies.

Dr. Di Donato was a Young Scientist at the XXXIII International Conference on Ground Penetrating Radar in 2010, and a Young Scientist Awarded at the XXX URSI General Assembly in 2011. He received an honorable mention from the IEEE - Antennas and Propagation Society Committee (Chapter Central and Southern Italy) in a Student Member best paper competition in 2012 and he was the recipient of the Latmiral Award by the Italian Electromagnetics Society (SIEm) in 2016.

Open Access funding provided by 'Università degli Studi di Catania' within the CRUI CARE Agreement